Investigations of Electronic Energy Transfer Dynamics in Multiporphyrin Arrays

Pierre Brodard, Stephan Matzinger, and Eric Vauthey*

Institut de Chimie-Physique de l'Université de Fribourg, Pérolles, CH-1700 Fribourg, Switzerland

Olivier Mongin, Cyril Papamicaël, and Albert Gossauer

Institut für Organische Chemie der Universität Freiburg, Pérolles, CH-1700 Fribourg, Switzerland

Received: February 16, 1999

A study of the dynamics of electronic energy transfer (EET) in arrays containing three, four, and six tetraphenylporphine units connected with phenylethynyl spacers is reported. For arrays containing the same chromophores, the EET rate constant was determined from the reorientational dynamics of the transition dipole using the crossed grating technique. EET time constants ranging from 150 ps up to 33 ns were measured, depending on the distance between the chromophores and on the metal ion complexed in the porphyrins. For the trimeric planar arrays, the interchromophoric distance varies by a factor of 2, while the ratio of the through space to through bond distances is constant. By comparing the measured EET rate constants with those calculated using Förster theory, the contributions of the Coulombic, through space, mechanism and of the exchange, through bond, mechanism could be estimated. For the arrays with the shortest spacer (through space distance of 23 Å), EET occurs through both exchange and Coulombic interactions with a ratio of about 3:1. This ratio increases up to about 10 as the distance is increased to 34.5 Å. At 46.5 Å, the ratio decreases and it appears that the Coulombic interaction becomes the dominant mechanism at longer distances. In the tetrahedral compound, the presence of a central saturated carbon strongly alters the electronic conducting properties of the spacer and makes the exchange mechanism inoperative.

Introduction

Over the past years, considerable efforts have been invested to synthesize and characterize molecular systems mimicking photosynthesis. Most of these investigations were focused on synthetic analogues of the reaction center, where the initial charge separation takes place.[1,2] However, the initial step of photosynthesis is light absorption and its overall efficiency depends primarily on that of this initial step and of the transfer of the excitation to the reaction center. In photosynthetic bacteria and in higher plants, this process takes place in light harvesting complexes, which are composed of thousands of pigment molecules that ensure a large absorption cross section over a broad spectral range. As such antennae have relatively large size, the excitation has to migrate over several pigments before being trapped at the reaction center. This trapping time has been measured to occur in less than 100 ps for several antenna complexes.[3,4] By considering this trapping time and the number of pigments in the antenna, it was concluded that a single electronic energy transfer (EET) step was occurring in a few hundred femtoseconds. This value was confirmed by direct measurements.[5,6]

So far, the synthesis of analogues of light harvesting systems has not received as much attention as the preparation of models of reaction centers. This might be due to the difficulty to synthesize large molecular assemblies, comprising many pigments arranged in a precise geometry. Indeed, the efficiency of natural antennae is due to an optimal arrangement of the pigments, which are covalently bound to a protein acting as a scaffolding. Most synthetic antennae are based on free base and metalloporphyrins.[7−11] In earlier systems, the porphyrin pigments were covalently bound through flexible bridges.[12−14] This leads to a large number of possible conformations with large differences in the interchromophoric distance and hence to a wide distribution of EET rate constants.

More recently prepared porphyrin arrays involve rigid spacers: when the pigments are directly linked by ethyne or butadiyne spacers, the absorption spectrum of the resulting array is substantially different from the sum of the absorption spectra of the individual pigments.[15−18] This is due to a strong electronic interaction between the chromophores via exciton coupling. Thus, the excitation is distributed over the whole array. If one wants to preserve the absorption spectra of the individual pigments, in order to cover a broad absorption range, it is preferable to use linkers with a poorer electronic conductivity. For example, Lindsey and co-workers have synthesized multiporphyrin arrays where the spacer is composed of an ethyne linkage between two aryl groups.[11] The absorption spectrum of the resulting arrays is almost a composite of the spectra of the individual chromophores. EET in porphyrin dyads composed of a Zn−tetraphenylporphine (ZnTPP) and of a free base tetraphenylporphine (FbTPP) was shown be as fast 24 ps. By comparing this value with the calculated time constant for Förster EET, the authors concluded that EET occurs mainly via a through bond (TB) electron exchange mechanism.

Indeed, contrary to singlet intermolecular EET that is known to take place predominantly via the through space (TS) dipole−dipole interaction, intramolecular EET can also occur through the exchange interaction (Dexter mechanism).[19] For example, Kroon et al. found that the distance and orientation dependence of EET in rigid bichromophoric molecules fitted neither a Förster

* To whom correspondence should be addressed. TEL: **41 (0)26300 8711. FAX: **41 (0)26300 9737. E-mail: Eric.Vauthey@unifr.ch.

10.1021/jp9905631 CCC: $18.00
Published on Web 07/14/1999

nor a Dexter model.[20] This was explained by a complex interplay between both mechanisms. The knowledge of the exact mechanism for such intramolecular EET processes is of course of primary importance for the design and the optimization of a synthetic antenna.

In this paper, we present an investigation of the EET dynamics in porphyrin arrays composed of three, four and six porphyrins with different metal ions (see Figure 1). In arrays containing identical chromophores, EET was monitored using the crossed grating (CG) technique. By varying the TB and the TS distances between the porphyrins, good insight into the contribution of both Coulombic and exchange mechanisms to the EET is obtained.

Experimental

Synthesis. The syntheses of tripodaphyrin[21,22] and benzene-centered porphyrin trimers[23] has been described earlier.

The larger trimer **4** was obtained in a two-step sequence. The zinc chelate **10**[22] was first reacted with an excess of 1,4-diiodobenzene in the presence of $Pd(PPh_3)_4$, leading to **11**, which was then coupled with 1,3,5-triethynylbenzene,[23,24] to give compound **4** (Scheme 1).

To achieve the synthesis of arrays with two different metallation states, such as **5**, **6**, and **8**, the use of 1,3,5-triethynylbenzene as starting material was inappropriate. Another core building block was needed with two different protecting groups of the terminal ethyne-C-atoms, enabling a stepwise synthesis. Reaction of **13a**[23] on its two iodine atoms with ethynyltriisopropylsilane yielded the desired core **13b**, the trimethylsilyl protecting group of which could be selectively cleaved with a stoichiometric amount of NaOH to give **13c** (Scheme 2). One equivalent (equiv) of the zinc chelate **14a** and its elongated analogue **14b** was first coupled with **13c** using palladium (0) as a catalyst, then the two remaining triisopropylsilyl groups were removed with fluoride ions, yielding **15a** and **15b**, respectively. The latter zinc complexes were finally reacted with 2 equiv of the free base porphyrins **12a** and **12d**, respectively, affording the corresponding $ZnFb_2$ porphyrin trimers **5** and **6**, respectively (Scheme 3). A similar strategy was employed to synthesize the Zn_2Fb_4 porphyrin hexamer **8**. Reaction of one equiv of the bifurcated Zn_2 dimer **16a**[23] with **13c** using triphenylarsine instead of triphenylphosphine as the ligand of the palladium catalyst, led to **17b** after cleavage of the triisopropylsilyl protecting groups. Cross coupling of Zn_2 dimer **17b** with 2 equiv of Fb_2 dimer **16b** under the same conditions gave the hexamer **8** containing two zinc and four free base porphyrins (Scheme 4).

Measurements. *Steady State Measurements.* Absorption spectra were measured on a commercial UV−vis−NIR spectrophotometer (Perkin-Elmer Lambda 2S). Fluorescence and fluorescence excitation spectra were recorded on a home-made fluorimeter.

Fluorescence Lifetime Measurements. The samples were excited by the second harmonic output at 532 nm of an active/passive mode-locked and Q-switched Nd:YAG laser (Continuum PY61-10). The pulse duration was 25 ps (fwhm) and the repetition rate 10 Hz. Fluorescence was measured at the magic angle polarization. A 100 mm monochromator was used for wavelength selection. Detection was achieved with a PIN silicon fast photodiode (Motorola MRD 500) connected to a 500 MHz, 2 GS/s digital oscilloscope (Tektronik TDS-620A). The response function of this system had a fwhm of 850 ps. Fluorescence lifetimes were obtained by iterative reconvolution of the response function with a single or a double exponential function.

Transient Grating (TG) Measurements. The picosecond TG setup has been described in details elsewhere.[25,26] The 25 ps pulses at 532 nm generated by the laser described above were split into three parts with relative intensities of 10:10:1. The two most intense pulses were crossed in the sample with an angle of about 1°. For probing, the weakest pulse was sent along a variable optical delay line before striking the grating at Bragg angle. The intensity of the diffracted pulse was measured with a vacuum photodiode. At each position of the delay line, the diffracted intensity was averaged over 10 laser pulses. For each measurement, the delay line was scanned 20 times. Each measurement was repeated three times. The polarization of the three beams was controlled using a combination of polarizer and half-wave plate. A precise polarization component of the signal could also be selected with a polarizer. For measuring population dynamics, the polarization of the two pump beams was parallel and that of the probe beam was at magic angle. The total pump intensity on the sample was about 0.5 mJ/cm^2. Probe light at 572 nm was generated by Raman shift in chloroform. The setup used to measure TG spectra has been described in ref 26. For polarization grating measurements, the polarization of the pump pulses were perpendicular as was the polarization of the signal with respect to the probe pulse.[27] In this case, the total pump intensity on the sample was about 2 mJ/cm^2.

Samples. Tetrahydrofuran (THF, Fluka), dimethylformamide (DMF, Fluka), and castor oil (CO, Fluka) were of the highest commercially available purity and were used without further purification. The concentrations of porphyrin arrays were adjusted to obtain an optical density at 532 nm of about 0.15 on 1 mm, the sample thickness. This corresponds to a concentration of the order of 10^{-4} M and to an average distance between two arrays of more than 250 Å, preventing the occurrence of intermolecular EET. During the experiments, the sample solutions were continuously stirred by N_2 bubbling. No sample degradation was observed after the measurements. All experiments were performed at 20 ± 1 °C.

Computation. The geometries of the trimers and the tetramer with FbTPP moieties were optimized using the AM1[28] method as implemented in the Gaussian 94 program.[29] For organic molecules, AM1 is known to produce structures that are in satisfactory agreement with experiment at a moderate computational cost. By choosing a semiempirical method, the difficult task to select an appropriately parameterized force field was avoided.

In order to obtain a better estimate for the structural errors, the AM1 and B3LYP/6-31G* structures of two representative building block molecules, i.e., one arm of compound **1** (fragment A) and tetraphenylmethane, the central part of compound **9** (fragment B), were compared. Gas phase geometries obtained by the B3LYP method in combination with the 6-31G* basis set are usually in excellent agreement with experiments. The B3LYP density functional method corresponds to a combination of Becke's three-parameter (B3) exchange functional[30] with the Lee−Yang−Parr correlation functional[31] as implemented in the Gaussian 94 package of programs.[29,32]

Both the AM1 and B3LYP/6-31G* reference method produced very similar structures for the fragment molecules. For the fragment A, the overall length obtained by AM1 differs by only ca. 0.5% from that calculated with the reference method. Larger errors were found for the torsion angle between the spacer and porphyrin, which is too small by ca. 6% in the AM1 geometry, due to an inherent underestimation of steric effects. This angle determines the relative orientation of donor and

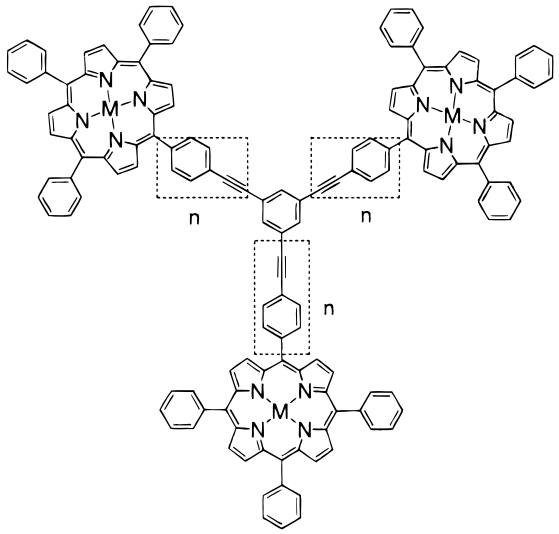

1 : M = 2H, n = 1
2 : M = Ni, n = 1
3 : M = Zn, n = 1
4 : M = Zn, n = 2
5 : M = Zn, 2H, 2H, n = 1
6 : M = Zn, 2H, 2H, n = 3
7 : M = Zn, Ni, 2H, n = 1

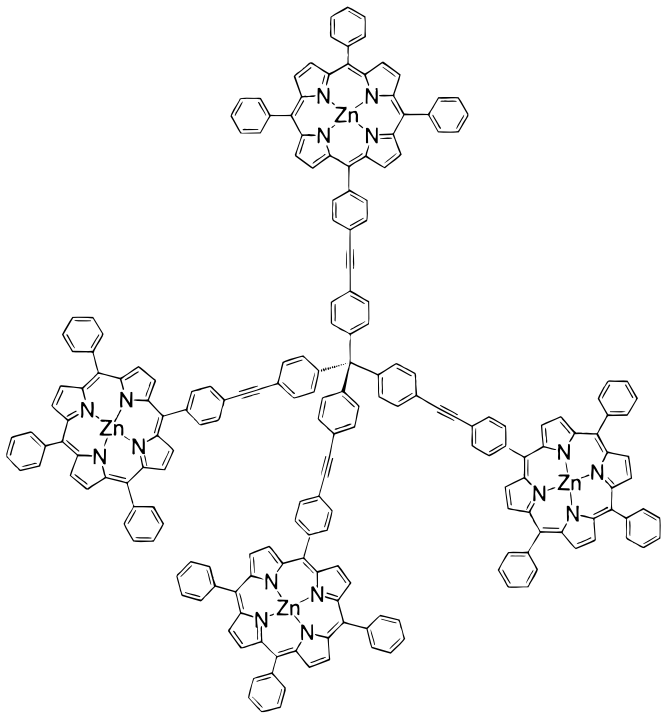

9

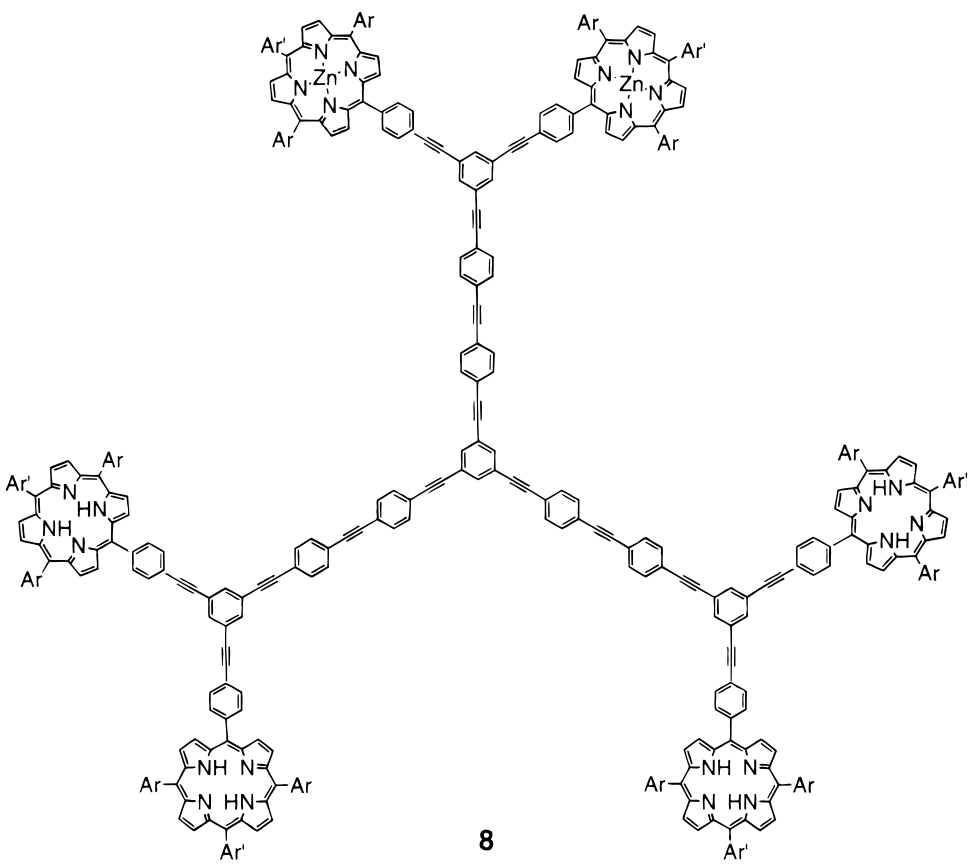

8

Ar= 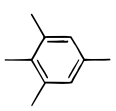

Ar'= 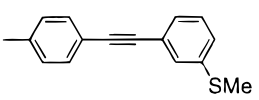

Figure 1. Nonoptimized structures of the multiporphyrin arrays.

SCHEME 1: Synthesis of All-Zn Porphyrin Trimer 4[a]

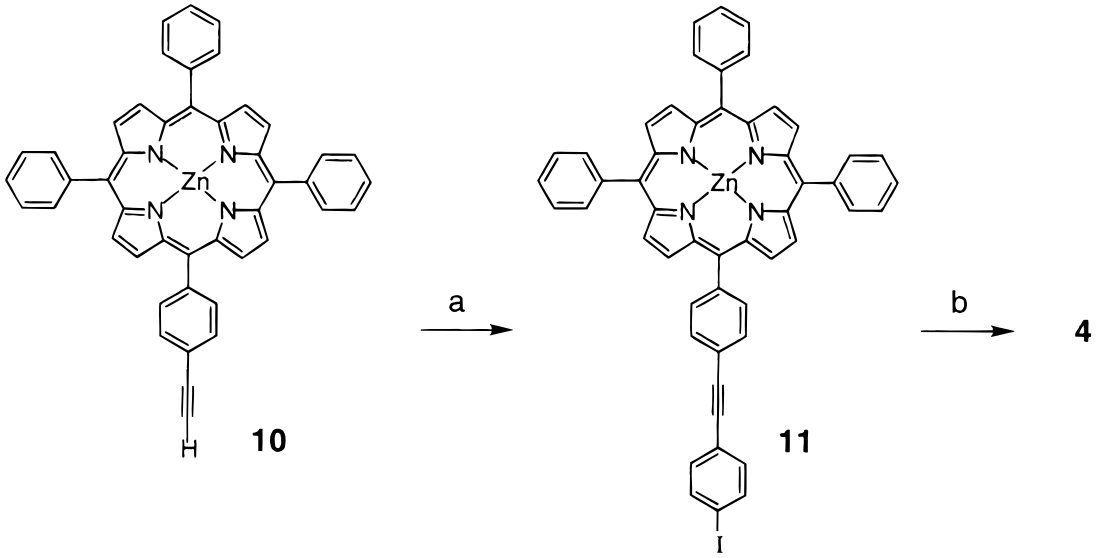

[a] Key: (a) 1,4-diiodobenzene, $Pd(PPh_3)_4$, DMF/Et_3N, 45 °C, 20 h (57%). (b) 1,3,5-triethynylbenzene, same conditions as those in (a) (41%).

SCHEME 2: Building Blocks for the Synthesis of $ZnFb_2$ Porphyrin Trimers 5 and 6[a]

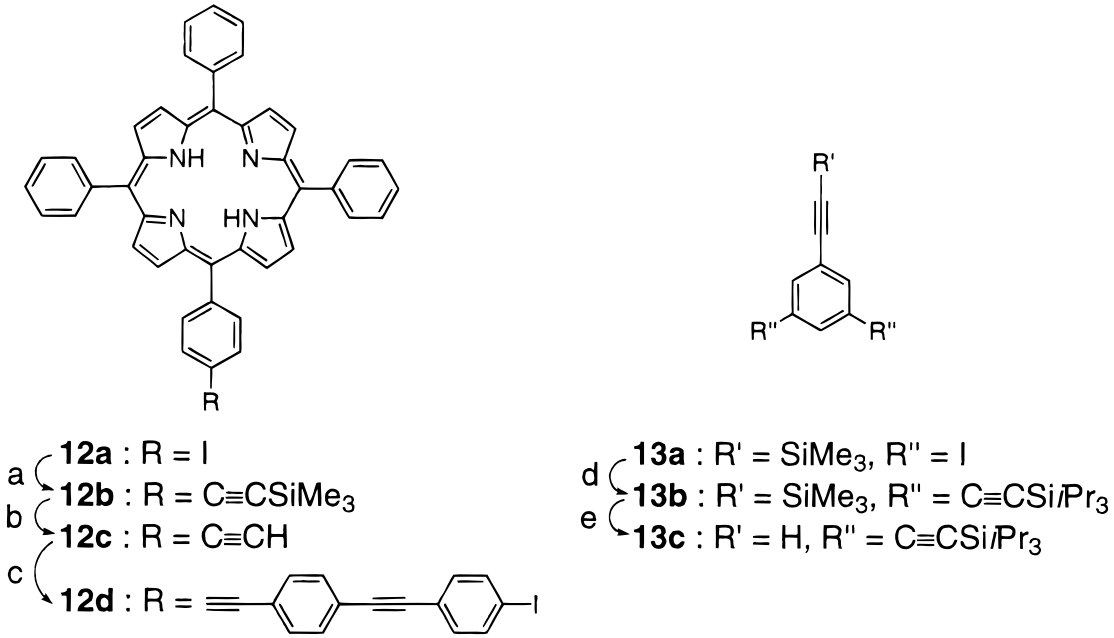

[a] Key: (a) $HC{\equiv}CSiMe_3$, $Pd(PPh_3)_4$, DMF/Et_3N, 40 °C, 20 h (82%). (b) NaOH, THF (89%). (c) 4,4′-diiodotolane, same catalyst and solvent as those in (a) 45 °C, 20 h (88%). (d) $HC{\equiv}CSi\textit{i}Pr_3$, $Pd(PPh_3)_4$, CuI, toluene/Et_3N, 40 °C, 2 h (97%). (e) 0.1 N NaOH, THF/EtOH (94%).

acceptor and thereby affects the calculated EET rate constants. In order to estimate the effect of solvent on the structure of fragment A, B3LYP/6-31G* calculations with an Onsager self-consistent reaction field as implemented in the Gaussian 94 program were performed. The resulting bond lengths and torsion angle in THF were the same, within less than 1%, as those in vacuum. For fragment B, only minor differences between the AM1 and the B3LYP/6-31G* structures were found.

Results

Steady State Measurements. The absorption spectrum of the arrays **1**−**9** is the composite of the spectra of the individual chromophores. A small red shift (≤5 nm) of the Soret band can nevertheless be noticed. Moreover, an additional band on the blue side of the Soret band that is not present in the composite spectrum can be observed. As its maximum is gradually shifted toward longer wavelengths as the length of the spacer is increased, this band can reasonably be assigned to the absorption of the linker. More details on the absorption spectra of the arrays **1**−**3** and **9** can be found in previous communications.[22,23] These absorption spectra indicate that the electronic interaction between the porphyrin moieties is weak.

The fluorescence spectra of arrays containing identical chromophores (**1**, **3**, **4**, and **9**) are the same as those of the individual porphyrins. Moreover, the fluorescence quantum yields are essentially equal. No fluorescence could be detected with compound **2**. This is not surprising as the monomer NiTPP is known to be nonfluorescent because of the presence of metal centered excited states below the porphyrin $S_1(\pi,\pi^*)$ state.[33] These states offer an efficient pathway for the nonradiative deactivation of NiTPP after excitation in the Q-band or in the Soret band.[34]

SCHEME 3: Synthesis of $ZnFb_2$ Porphyrin Trimers 5 and 6[a]

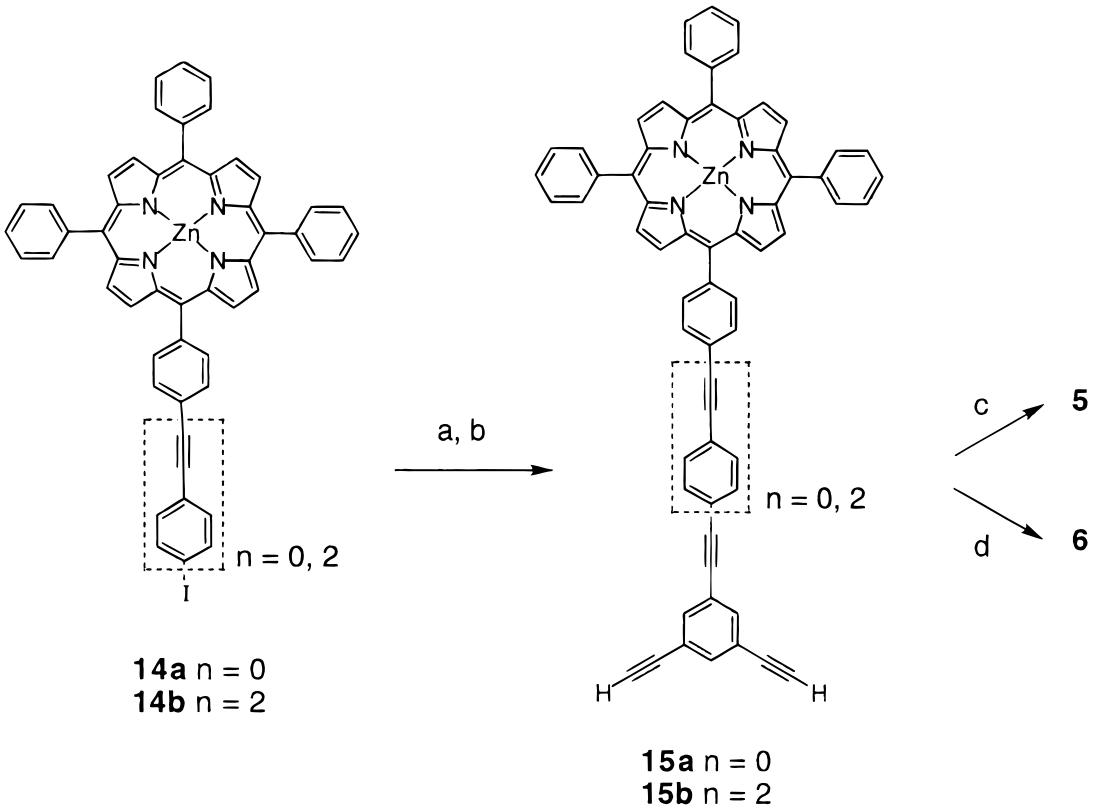

[a] Key: (a) **13c**, $Pd(PPh_3)_4$, DMF/Et_3N, 45 °C, 20 h (73% for a, 85% for b); (b) TBAF, THF (99% for **15a**, 98% for **15b**); (c) **12a**, same conditions as those in (a) (79%); (d) **12d**, same conditions as those in (a), 40 h (37%).

SCHEME 4: Synthesis of Zn_2Fb_4 Dentritic Porphyrin Hexamer 8[a]

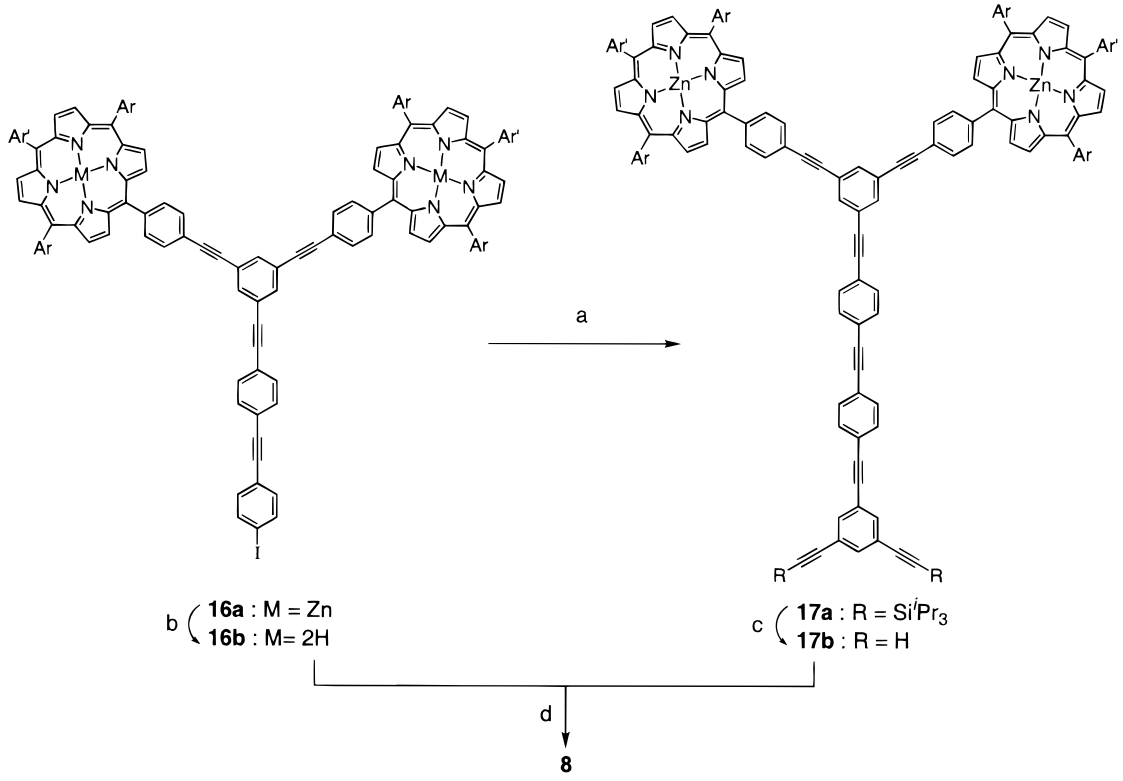

[a] Key: (a) **13c**, Pd_2dba_3, $AsPh_3$, DMF/Et_3N, 30 °C, 5 h (44%); (b) TFA, $CHCl_3$ (74%); (c) TBAF, THF (73%); (d) **17b** (1 equiv), **16b** (2 equiv), same conditions as those in (a) (19%).

In the case of arrays with different chromophores (**5**−**8**), the fluorescence spectrum depends on the interchromophoric distance. These distances, obtained from AM1 calculations, are listed in Table 1. For compound **5**, where the interchromophoric

TABLE 1: Center to Center through Space Distances R_{TS} and through Bond Distances R_{TB} between the Chromophores, Determined from the AM1 Structures[a]

array	R_{TS} (Å)	R_{TB} (Å)
trimers **1**, **2**, **3**, **5**, **7**	23.0	26.5
trimer **4**	34.5	40.0
trimer **6**	46.5	53.5
tetramer **9**	D_{2d} (S_4)	32.0
P_1-P_2	24.6 (25.6)	
P_1-P_3	27.1(26.6)	
P_1-P_4	27.1(26.6)	
P_2-P_3	27.1(26.6)	
P_2-P_4	27.1(26.6)	
P_3-P_4	24.6(25.6)	
hexamer **8**		
ZnTPP−FbTPP	35.5	67.5
ZnTPP−ZnTPP	23.0	26.5

[a] For compound **9**, the values between brackets are for the S_4 structure.

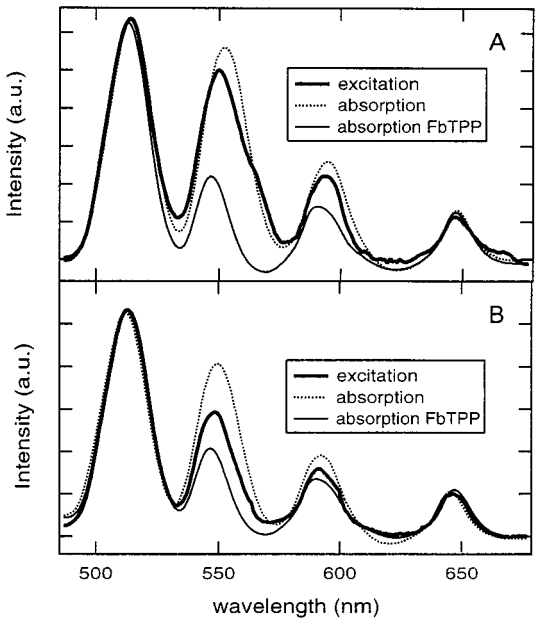

Figure 2. Absorption and fluorescence excitation spectra at 720 nm of trimers **5** (A) and **6** (B) together with the absorption spectrum of FbTPP in THF (intensity in arbitrary units, au).

distance is the shortest, the fluorescence spectrum is essentially the same as that of FbTPP, irrespective of the excitation wavelength. As shown in Figure 2A, the fluorescence excitation spectrum measured at 720 nm, where the emission is due to the FbTPP moiety only, is almost identical to the absorption spectrum of the array, indicating a very efficient excitation transfer from ZnTPP to FbTPP. In the case of compounds **6** and **8**, where the interchromophoric distance is substantially longer, the fluorescence spectrum depends on the excitation wavelength. Excitation at 570 nm, where absorption by ZnTPP dominates, results in a fluorescence spectrum that contains both ZnTPP and FbTPP bands. Moreover, the contribution of the ZnTPP band in the fluorescence excitation spectrum at 550 nm, is substantially weaker than in the absorption spectrum (see Figure 2B). Thus, EET in **6** and **8** is clearly less efficient than in **5**. Finally, the fluorescence spectrum of compound **7** is very similar to that of array **5**. Moreover, the fluorescence excitation spectrum at 720 nm does not contain any clear feature, which could be ascribed to NiTPP. This indicates that EET from ZnTPP to FbTPP takes place and that NiTPP does apparently not play any significant role.

TABLE 2: Fluorescence Lifetimes τ_{fl} Excited State Population Decay Times τ_{pop} in THF, Polarization Anisotropy Decay Times τ_r, and Initial Polarization Anisotropies r_0 in CO[a]

array	τ_{fl} or τ_{pop} (ns)	τ_r (ns)	r_0 (±0.005)
1	12.0[b]	0.310	0.16
2	0.250[c]	>2.5	0.10
3	1.82[b]	0.075	0.10
4	1.82[b]	0.260	0.10
5 (ZnTPP*)	0.073[c]		
6 (ZnTPP*)	1.54[b]		
7 (FbTPP*)	8.8[b]		
8 (ZnTPP*)	1.49[b]		
9	1.82[b]	0.130	0.10

[a] For compounds containing different porphyrins, the chromophore that was monitored is indicated between brackets. [b] τ_{fl}. [c] τ_{pop}.

TABLE 3: Calculated Spectral Overlap Integrals J_F and Average Orientational Factors κ^2 for Various D/A Pairs

array	D → A	J_F (10^{-14} cm^6 mmol^{-1})	κ^2
1	FbTPP → FbTPP	2.51	1.35
3,4	ZnTPP → ZnTPP	3.38	1.35
5,6	ZnTPP → FbTPP	3.54	1.35
8	ZnTPP → FbTPP	3.54	0.58
9 (D_2d)	ZnTPP → ZnTPP	3.56	
	$P_1 \rightarrow P_2$		1.16
	$P_1 \rightarrow P_3$		1.21
	$P_1 \rightarrow P_4$		0.98
	$P_2 \rightarrow P_3$		1.10
	$P_2 \rightarrow P_4$		1.54
	$P_3 \rightarrow P_4$		1.84

Time-Resolved Measurements. Time-resolved measurements have been performed in order to get better information on the dynamics of EET within these arrays. Two techniques have been used: (i) for processes with a rate constant inferior to 1 ns^{-1}, fluorescence lifetime measurements were performed, and (ii) for measuring faster processes, the population dynamics of the excited state was measured using the TG technique. Moreover, for monitoring the excitation transfer in arrays containing identical chromophores, the CG technique was applied. These two techniques will be described in more detail below.

Fluorescence Lifetime Measurements. The fluorescence lifetimes of arrays composed of ZnTPP only in THF (compounds **3**, **4**, and **9**) were identical, within the experimental error, to the fluorescence lifetime of ZnTPP monomer, and amount to 1.82 ± 0.08 ns in THF. Similarly, the fluorescence lifetime of both array **1**, containing three FbTPP chromophores, and FbTPP itself amounted to 12.0 ± 0.1 ns in THF. These values confirm that the electronic interaction between the chromophores is weak.

For arrays containing both ZnTPP and FbTPP (compounds **5**−**8**), the fluorescence lifetime of the ZnTPP excited moiety was shorter than that of the monomer. For arrays **5** and **7**, it was too short to be measured with this technique. The fluorescence lifetimes of ZnTPP* in compounds **6** and **8** are listed in Table 2. For arrays containing ZnTPP and FbTPP only, the decay of the fluorescence originating from the FbTPP* moiety was identical to that of the monomer. This indicates that the EET in these arrays is vectorial and proceeds from ZnTPP to FbTPP. This result is in agreement with measurements performed with other types of porphyrin arrays.[35,11] The situation is more complex for compound **7**, which additionally contains a NiTPP chromophore. In this case, the lifetime of the FbTPP fluorescence is shorter and amounts to 8.8 ns. This shows that NiTPP offers a new channel for the deactivation of FbTPP*.

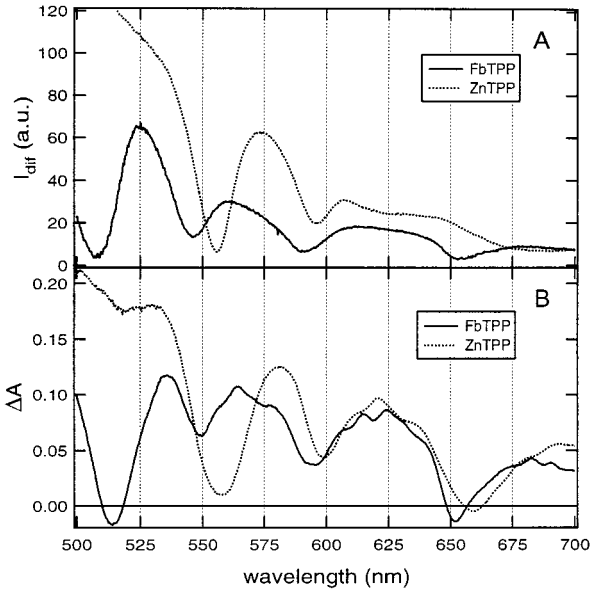

Figure 3. (A) TG spectra and (B) TA spectra obtained 50 ps after excitation at 355 nm of ZnTPP and FbTPP in THF.

TG Measurements. The principle of the TG technique has been described in detail in several reviews.[36,37] In brief, the sample is excited by two time coincident pump pulses, which interfere in the sample. The resulting grating-like modulation of excitation intensity results into spatial distributions of ground state, excited state and/or photochemical intermediate and product concentrations. Therefore, similar grating-like modulations of absorbance and refractive index, also called amplitude and phase gratings, are generated. The amplitudes of these absorbance and refractive index distributions, ΔA and Δn, respectively, can be probed by a third laser pulse striking the grating at Bragg angle θ_B. The intensity of the light diffracted from these gratings I_{dif} is related to ΔA and Δn through the following equation:[38]

$$\frac{I_{dif}(\lambda_{pr})}{I_{pr}(\lambda_{pr})} \cong \exp\left(-\frac{A(\lambda_{pr})\ln 10}{2\cos\theta_B}\right)\left[\left(\frac{\Delta A(\lambda_{pr})\ln 10}{4\cos\theta_B}\right)^2 + \left(\frac{\Delta n(\lambda_{pr})\pi d}{\lambda_{pr}\cos\theta_B}\right)^2\right] \quad (1)$$

where I_{pr} is the intensity of the probe pulse, A is the average absorbance at the probe wavelength λ_{pr}, and d is the sample thickness. Both ΔA and Δn are proportional to the photoinduced concentration changes ΔC and therefore the time dependence of diffracted intensity is given by

$$I_{dif}(t) \propto \Delta C(t)^2 \quad (2)$$

Because the TG technique is a zero background method, one of its advantages over the more conventional transient absorption (TA) spectroscopy is its superior sensitivity.

Figure 3A shows the TG spectra measured with ZnTPP and FbTPP in THF, 50 ps after excitation at 355 nm. The probe pulse was a white light pulse, generated by self-phase modulation. Therefore, these spectra correspond to the square of the absorption spectrum plus the square of the dispersion spectrum of the transient.[26] The major drawback of the TG technique is the lack on information on the sign of ΔA and Δn. It can be indeed difficult to known from a TG spectrum whether one monitors the excited state population, the ground state one or both. This information can be obtained by performing TA measurements or heterodyne TG.[39] The TA spectra shown in Figure 3B have been obtained by measuring the intensity of the transmitted probe pulse. These spectra, which are very similar to those reported by Holten et al.,[40] indicate that the diffracted intensity obtained by probing at 532 and 572 nm (vide infra) is dominated by the contribution of the excited state population.

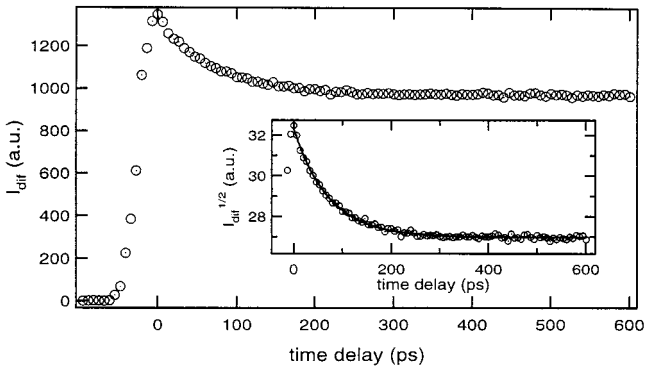

Figure 4. Time evolution of the diffracted intensity at 572 nm after excitation at 532 nm of compound **5** in THF. Inset: decay of the square root of the diffracted intensity and best single exponential fit.

Figure 4, shows the time profile of the diffracted intensity at 572 nm after excitation of compound **5** at 532 nm. The probe pulse at 572 nm monitors both ZnTPP* and FbTPP* population. The extinction coefficients of ZnTPP and FbTPP at 532 nm are almost identical.[41] Thus, the excited state population directly after excitation of compound **5** comprises 1/3 of ZnTPP* moieties and 2/3 of FbTPP* moieties, while after EET, the excited state population consists of FbTPP* only. As the TG intensity of ZnTPP* at 572 nm is larger than that FbTPP* (see Figure 3A), the initial exponential decay observed in Figure 4 corresponds to the EET from ZnTPP* to FbTPP. The insert shows the square root of the diffracted intensity that is directly proportional to concentration changes. This decay can be fitted with a single exponential function. The resulting decay time is listed in Table 2.

TA and TG spectra measured with arrays containing identical porphyrins (compounds **1**−**4** and **9**) show the same features upon excitation at 355 nm as those of the individual chromophores. For ZnTPP and arrays containing ZnTPP only (compounds **3**, **4**, and **9**), the decay of the diffracted intensity at 532 nm is biphasic. The faster component with a decay constant of 5.5×10^8 s^{-1}, corresponds the S_1 population, which decays to S_0 through fluorescence and internal conversion and to T_1 through intersystem crossing (ISC). The slower component corresponds to the T_1 population decaying in the μs time scale. For FbTPP and array **1**, the decay of the diffracted intensity at 532 nm is too slow relatively to the time window of the TG setup (between 0 and 5 ns) to be measured accurately. This is not surprising in view of the long S_1 lifetime of FbTPP. Finally, for NiTPP and for array **2**, the lifetime of the excited state population amounts to 250 ± 12 ps. This lifetime corresponds to the decay of a metal-centered (d,d) excited state.[34] The decay to this state in less than 350 fs from the $S_1(\pi,\pi^*)$ state is responsible for the lack of fluorescence of NiTPP.[42]

CG Measurements. CG measurements have been performed to obtain information on EET in arrays composed of identical chromophores (compounds **1**−**4** and **9**). In a CG experiment, the pump pulses have perpendicular linear polarization. Although the excitation intensity in the intersection region is uniform, the polarization of the pump light is spatially modulated.[43] Such a polarization grating can be described as the sum

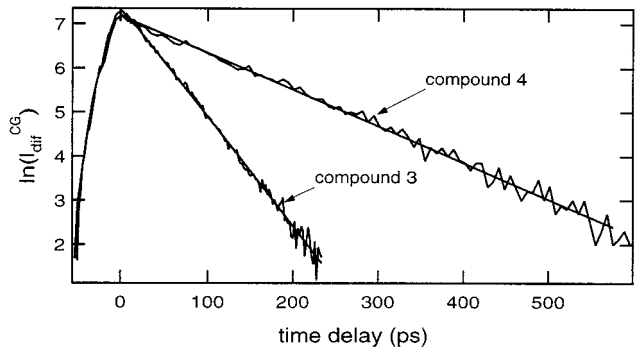

Figure 5. Logarithmic plot of the diffracted intensity measured at 532 nm in the CG geometry with compounds **3** and **4** in CO and best linear fit.

of four intensity gratings with +45° and −45° linear polarization and with left and right circular polarization.[44] The two latter gratings can be neglected when working with optically inactive molecules. Upon absorption by the sample, the population is uniform, but the orientation of the excited molecules is spatially modulated. This modulated orientational anisotropy gives rise to modulations of dichroism and birefringence, which act as a half-wave plate, i.e., if the polarization of the probe beam makes an angle ϕ_{pr} relative to the polarization of one of the pump pulse, the polarization of the diffracted pulse will be at an angle ϕ_{dif} relatively to this pump pulse:

$$\phi_{dif} = \arctan\left[\frac{\cos(\phi_{pr} - 45)}{\cos(\phi_{pr} + 45)}\right] + 45 \qquad (3)$$

In most cases, the polarization of the probe pulse is parallel to one of the pump pulse. Thus, the polarization of the diffracted pulse is rotated by 90° relative to that of the probe pulse.

Such dichroism and birefringence gratings can decay by both population relaxation and reorientation of the transition dipoles,[45] thus

$$I_{dif}^{CG}(t) \propto [\Delta C(t) r(t)]^2 \qquad (4)$$

where $r(t)$ is the time dependence of the anisotropy.

If the anisotropy decay is much faster than the population relaxation, the time profile of the diffracted intensity reflects directly $r(t)$. Otherwise, the anisotropy can be obtained from the ratio of the time profile measured with the CG geometry (eq 4) with the time profile measured with conventional TG (eq 2).

The anisotropy decay occurs through reorientation of the transition dipole. For the porphyrin arrays investigated here, this can take place by EET from one porphyrin moiety to another, by rotational diffusion of the whole array and also by internal rotation of the TPP groups in the array. These two diffusional processes can be strongly slowed down by working in a highly viscous solvent such as castor oil (CO, $\eta = 6-8$ P).

Figure 5 shows the time profiles of the diffracted intensity measured in the CG experiment with compounds **3** and **4** in CO. Because the decay time is much faster than that of the excited state population, these profiles corresponds to the anisotropy decay. The measured anisotropy decay times τ_r in CO are listed in Table 2. These measurements have been repeated in THF and in DMF which have a much lower viscosity. For compound **3**, τ_r is independent of the solvent. For compound **4**, a slight decrease of the decay time with decreasing viscosity was observed, indicating a small contribution of diffusional reorientation in low viscosity solvents. As a comparison, the anisotropy decay time measured with the ZnTPP monomer in THF amounts to 160 ps. Thus, as the arrays are more than three times more voluminous than ZnTPP, a lower limit of about 600 ps can be estimated from the Stokes−Einstein−Debye equation for the rotational time of compound **3** in THF. Moreover, the rotational time of ZnTPP in CO can be estimated to be larger than several tens of nanoseconds. Consequently, the anisotropy decays measured in CO do not contain any contribution from diffusional reorientation.

CG measurements have also been performed with compounds **1**, **2**, and **9**. For all compounds, the time profiles could be satisfactorily fitted using a single exponential function decaying to zero. For the array **2**, the decay of the diffracted intensity measured with the CG geometry is the same, within the experimental error, as that measured with the conventional TG geometry. Therefore, a lower limit of 2.5 ns can be estimated for the decay time of the anisotropy with this array. For all the other compounds, the decay of the diffracted intensity was much faster than the decay of the population.

The CG technique allows the anisotropy changes to be measured with a high signal/noise ratio, but the absolute value of the anisotropy at time zero r_0 cannot be obtained directly. However, r_0 can be determined by comparing the initial intensity of the signal measured using pump and probe pulses with parallel polarization $I_{dif}^{||}(0)$ with the initial intensity measured using the CG geometry $I_{dif}^{CG}(0)$:[45]

$$r_0 = \frac{2I_{dif}^{CG}(0)^{1/2}}{3I_{dif}^{||}(0)^{1/2} - 4I_{dif}^{CG}(0)^{1/2}} \qquad (5)$$

The values of r_0 are also listed in Table 2.

Discussion

Relationship between the Measured Decay Times and the EET Rate Constants. *Arrays Containing Identical Chromophores.* The initial anisotropy depends on the angle γ between the transition dipole moment involved in the pump process and that involved in the probe process:

$$r_0 = \frac{2}{5} P_2[\cos(\gamma)] \qquad (6)$$

where $P_2(x)$ is the second Legendre polynomial. This expression is only valid in the so-called dephased limit. At times shorter than the electronic dephasing time, r_0 can be as large as 1.[46] However, in liquids at room temperature, this electronic dephasing time is typically of the order of a few tens of femtoseconds, thus eq 6 is perfectly valid for the present investigation.

For arrays containing only ZnTPP or NiTPP chromophores, the initial anisotropy amounts to 0.1 as it is for an individual ZnTPP molecule. This value is due to the fact that the excited state is doubly degenerate and can be populated via two perpendicular transition dipoles (Q_x and Q_y). Indeed, the transition dipole for the probe process can be either parallel ($r_0 = 0.4$) or perpendicular ($r_0 = -0.2$) to the transition dipole involved in the excitation process. Consequently, the average initial anisotropy amounts to 0.1. This value is only reached after equilibration between the degenerate excited states. Hochstrasser and co-workers have determined that this process occurs in 350 fs for a Zn−porphyrin derivative.[18]

The excited state of FbTPP is no longer degenerate because of the symmetry lowering introduced by the two central protons. Moreover, proton tautomerism at room temperature takes place

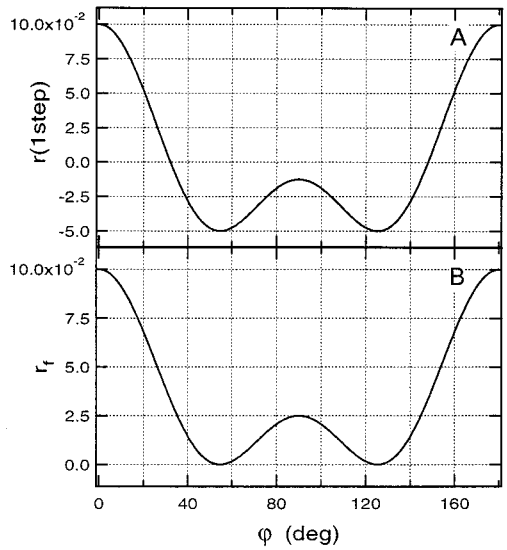

Figure 6. Polarization anisotropy in compounds **3** and **4** (A) after a single EET step and (B) after randomization of the excitation r_f as a function of the twist angle φ.

in about 200 μs and cannot lead to a decay of the anisotropy in the time scale considered here.[47] The departure from the theoretical value of $r_0 = 0.4$ at 532 nm can be explained by the unequal contribution of both Q_x and Q_y transition dipoles to the absorption at this wavelength. This is in agreement with emission polarization measurements reported by Borisevitch et al., which have revealed that the polarization anisotropy of the fluorescence of FbTPP at 646 nm upon excitation at 532 nm is neither 0.4 nor -0.2 but amounts to about 0.18.[48]

The CG measurements carried out with compounds **1**, **3**, **4**, and **9** show that the anisotropy decays to zero in a medium where diffusional reorientation is inhibited. This decay is due to the reorientation of the transition dipole accompanying EET from one chromophore to another. The reduction of the anisotropy upon a single EET step strongly depends on the relative orientation of the porphyrins in the array. For example, if the arrays **3** and **4** were planar, EET would not be accompanied by an anisotropy change. Indeed, the angles between one transition dipole of the initially excited porphyrin (P_1) and the transition dipoles of a neighbor porphyrin (P_2 or P_3) are 120° and 30°. From eq 6 this results into anisotropies of -0.05 and 0.25, respectively, which give an average value of 0.1. This calculation has been repeated for various twist angles φ between the porphyrin plane and the plane formed by the spacer. Figure 6A shows the polarization anisotropy after a single EET step as a function of φ, assuming that all the porphyrins are twisted in the same direction, i.e., assuming a D_3 symmetry. This figure shows that small departures from planar configuration (i.e., from $\varphi = 0$) lead to a substantial decrease of r.

According to AM1 calculations with the trimeric array **1**, the porphyrins are twisted at an angle of 64° (see Figure 7A). Thus, the anisotropy after a single EET step should become negative. However, as these arrays are composed of identical chromophores, the excitation is never trapped and further EET processes, either toward a third porphyrin or back on the initially excited one P_1 can take place. Consequently, the time dependencies of the excited state population of P_1 and of those of the two neighbor porphyrins P_2 and P_3 are

$$P_1^*(t) = \frac{P_1^*(0)}{3}[1 + 2\exp(-3k_{EET}t)] \qquad (7a)$$

$$P_{2,3}^*(t) = \frac{P_1^*(0)}{3}[1 - \exp(-3k_{EET}t)] \qquad (7b)$$

These equations show that, after a few EET steps, the probability of finding the excitation on any of the three chromophores is identical. Thus the final anisotropy r_f can be easily determined. Figure 6B shows r_f calculated as a function of the twist angle φ. The anisotropy after randomization of the excitation varies between 0.1 for a planar array to 0 for a twist angle of 55° or 125°. At 64°, r_f amounts to 0.004, a value that can experimentally not be differentiated from zero. In liquids at room temperature, a distribution of this angle around 64° can be expected, because the potential energy surface along this coordinate is very shallow. Consequently, the measured r_f is in agreement with the above calculations.

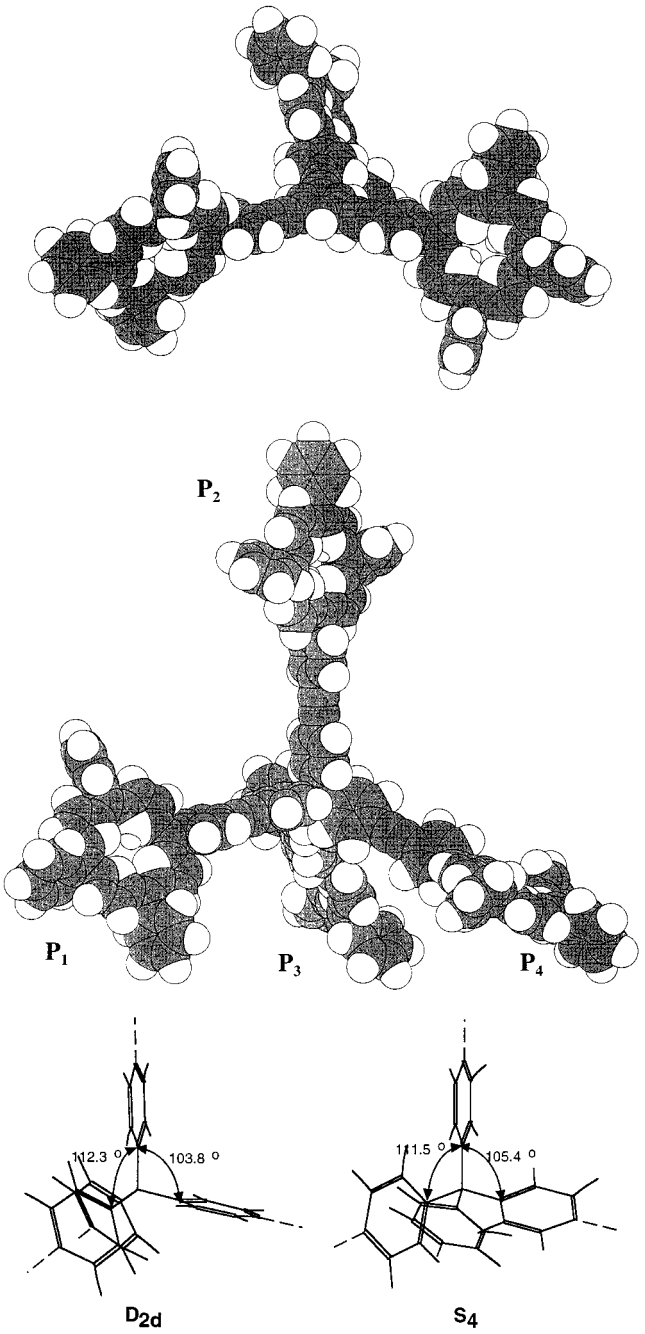

Figure 7. AM1 geometry of compounds **1** (A) and **9** (B, D_{2d} structure with free base porphyrins). (C) Details of tetraphenylmethane core of the two AM1 structures of compound **9**.

In summary, this model indicates that the anisotropy decays from an initial value of $r_0 = 0.1$ to a final value $r_f \approx 0$ with a time constant $\tau_r = (3k_{EET})^{-1}$. The EET rate constants calculated from the anisotropy decay of compounds **3** and **4** are listed in Table 4.

In the trimer **1**, the symmetry is lower than in the trimers **3** and **4**, and the anisotropy decay after a single EET step depends on the relative position of the central protons in the three FbTPP chromophores. However, the initial anisotropy value $r_0 = 0.16$ indicates that both Q_x and Q_y transition dipoles contribute to the absorption at 532 nm. Therefore, the dependence on the twist angle φ of the anisotropy after a single EET should not be significantly different from that calculated for compounds **3** and **4**.

Furthermore, if one assumes that the EET rate constant does not depend on the relative position of the central protons, the time constant for EET also amounts to one-third of the anisotropy decay time. This assumption implies that EET does not depend on the relative angles between the transition dipoles, hence that EET proceeds through an exchange mechanism only. The validity of this hypothesis will be discussed in more details in the next section.

Similar assumptions on the EET mechanism have to be made to interpret the anisotropy decay measured with the tetramer **9**. Both AM1 and B3LYP/6-31G* calculations on tetraphenylmethane (TPM), the central part of compound **9**, result into two structures, having D_{2d} and S_4 symmetry, with an energy difference of less than 1 kcal/mol. The TPM core is unchanged in the AM1 structure of the whole molecule. These two structures will be called D_{2d} and S_4 according to the symmetry of the central TPM core.

The angles between the branches are 112.3° and 103.8° for the D_{2d} structure (see Figures 7B and C) and 111.5° and 105.4° for the S_4 structure (see Figure 7C). Consequently, there are, in both cases, two different TS distances between one ZnTPP moiety and its three neighbors (see Table 1). In the D_{2d} geometry, each chromophore has one neighbor at 24.6 Å and two neighbors at 27.1 Å. The same holds for the S_4 structure, but the distances are 25.6 and 26.6 Å, respectively. Thus, if EET occurs through the Förster mechanism, two different EET rates can be expected for both geometries. In this case, the time evolution of the excited state population of the various chromophores is

$$P_1^*(t) = \frac{P_1^*(0)}{4}[1 + \exp(-4k_l t) + 2\exp(-2(k_l + k_s)t)] \quad (8a)$$

$$P_2^*(t) = \frac{P_1^*(0)}{4}[1 + \exp(-4k_l t) - 2\exp(-2(k_l + k_s)t)] \quad (8b)$$

$$P_{3,4}^*(t) = \frac{P_1^*(0)}{4}[1 + \exp(-4k_l t)] \quad (8c)$$

were k_l and k_s are the rate constants for long distance and short distance EET, respectively. After a few EET steps, the probability of finding the excitation on any of the chromophores amounts to 0.25. The final anisotropy value after randomization of the excitation r_f calculated using the parameters from the AM1 structure amounts to 0.028 and 0.023 for the D_{2d} and the S_4 structures, respectively. This final value is reached after a biexponential decay of the anisotropy with rate constants of $4k_l$ and $2(k_l + k_s)$.

TABLE 4: Rate Constants of EET k_{EET} Calculated from the Data Listed in Table 2, Rate Constants of EET via the Dipole−Dipole Interaction k_C Calculated with eq 11, and Rate Constants of EET via the Exchange Interaction k_E Calculated as $k_E = k_{EET} - k_C$

array	D → A	k_{EET} (ns^{-1})	k_C (ns^{-1})	k_E (ns^{-1})	k_E/k_C
1	FbTPP → FbTPP	1.07	0.49	0.58	1.2
2	NiTPP → NiTPP	<0.1			
3	ZnTPP → ZnTPP	4.44	1.37	3.07	2.25
4	ZnTPP → ZnTPP	1.28	0.11	1.17	10.6
5	ZnTPP → FbTPP	6.57	1.43	5.14	3.6
6	ZnTPP → FbTPP	0.05	0.01	0.04	4
7	FbTPP → NiTPP	0.03			
	ZnTPP → NiTPP	0.3−1.5			
8	ZnTPP → FbTPP	0.062[a]	0.043	0.019[b]	0.45
9 (D_2d)	ZnTPP → ZnTPP	1.92			
	$P_1 \rightarrow P_2$		0.76		
	$P_1 \rightarrow P_3$		0.44		
	$P_1 \rightarrow P_4$		0.36		
	$P_2 \rightarrow P_3$		0.41		
	$P_2 \rightarrow P_4$		0.56		
	$P_3 \rightarrow P_4$		1.20		

[a] Calculated as $k_C + k_E$. [b] Calculated with eq 10.

On the other hand, the TB distances between the various chromophores are equal and, if EET occurs via the Dexter mechanism, the various EET paths should have similar efficiencies. In this case, the decay time of the anisotropy should correspond to about $(4k_{EET})^{-1}$.

Arrays Containing Two Different Chromophores. The interpretation of the time profiles measured with arrays containing two different chromophores is straightforward. These kinetics correspond to the decay of the excited state concentration of the energy donor (D) which takes place through intersystem crossing (ISC), internal conversion (IC), fluorescence, and EET. Thus the observed rate constant (k_{fl} or k_{pop} in Table 2) is equal to

$$k_{obs} = k_{ISC} + k_{ic} + k_{rad} + mk_{EET} = k_{S_1} + mk_{EET} \quad (9)$$

where k_{ISC}, k_{ic}, and k_{rad} are the rate constant for ISC, IC, and radiative deactivation of D, respectively, k_{S_1} is the rate constant for the decay of S_1 state of D in the absence of EET. The m on the right-hand side of eq 9 represents the number of equivalent energy acceptor (A) chromophores, where the excitation can migrate in a single EET step from D. For compounds **5** and **6**, there are two A porphyrins, thus $m = 2$.

The interpretation of the decay measured with the hexamer **8** depends on the EET mechanism. If EET takes place via a TS mechanism, it will predominantly occur to the FbTPP molecule which is the closest to the ZnTPP donor. In this case, m in eq 9 is equal to unity. However, if EET occurs via a TB mechanism, m amounts to 4 as all the TB paths between a ZnTPP and a FbTPP moiety are equivalent. If both contributions are operative, eq 9 becomes

$$k_{obs} = k_{S_1} + k_C + 4k_E \quad (10)$$

where k_C is the rate constant for TS EET via Coulombic interaction and k_E is the rate constant for TB EET, via exchange interaction.

Compounds Containing Three Different Chromophores. The EET dynamics in the trimer **7** was not measured directly, as it was not possible to find a probe wavelength corresponding to the absorption of a single chromophore only. However, EET from the ZnTPP to the FbTPP moiety should proceed with the same rate constant as in compound **3**, because both the TS and

the TB distances are identical (see Table 1). The rate constant of EET from ZnTPP to NiTPP can be estimated with this value and with the quantum yield of fluorescence of the ZnTPP moiety ($\Phi_{fl} = 0.004$).[23] Table 4 shows that EET between ZnTPP and NiTPP indeed takes place, but the error on the rate constant is large. This is due to the uncertainty on the fluorescence quantum yield.

The decrease of the observed fluorescence lifetime of the FbTPP chromophore in array **7** relatively to that measured with FbTPP alone, indicates that EET from FbTPP to NiTPP is operative. On the other hand, EET processes from NiTPP can be expected to be rather inefficient, due to its short excited lifetime and because of the energy of its lowest singlet excited state, which has recently been determined to lie 1.18 ± 0.13 eV above the ground state.[49] This low energy makes EET to both ZnTPP and FbTPP endothermic by more than 0.7 eV, and thus extremely improbable.

EET Mechanism. The above discussion shows that, in some cases, the knowledge of the EET mechanism is required to extract the EET rate constants from the measured decay times. In general, EET can proceed via both the Coulombic dipole−dipole interaction (Förster mechanism) and the exchange interaction (Dexter mechanism), i.e. $k_{EET} = k_C + k_E$.

The rate constant of Förster EET k_C is given by[50]

$$k_C = \frac{8.8 \times 10^{-25} \kappa^2 \Phi_{fl}}{n^4 R^6 \tau_{fl}} J_F \qquad (11a)$$

$$J_F = \frac{\int F_D(\nu)\epsilon_A(\nu)\nu^{-4} d\nu}{\int F_D(\nu)} \qquad (11b)$$

where n is the refractive index of the medium, R is the center to center distance between D and A, Φ_{fl} is the fluorescence quantum yield of D (Φ_{fl}(ZnTPP*) = 0.033,[51] Φ_{fl}(FbTPP*) = 0.11),[52] J_F is the spectral overlap integral, and $F_D(\nu)$ and $\epsilon_A(\nu)$ are the intensities of the D fluorescence and A absorption spectra, respectively. Finally, κ is a dipole−dipole orientation factor:

$$\kappa = \sin\theta_D \sin\theta_A \cos\phi - 2\cos\theta_D \cos\theta_A \qquad (12)$$

where θ_D and θ_A are the angles between the transition dipoles of D and A and the internuclear D−A axis, respectively, and ϕ is the azimuthal angle between the transition dipoles of D and A. EET through the Förster mechanism is a TS process, whose efficiency depends on the magnitude and relative orientation of the transition dipoles of D and A.

The rate constant of exchange EET k_E is given by[53]

$$k_E = \frac{4\pi^2 (H^0_{DA})^2 \exp[-\beta_{EET}(R - R_0)]}{h} + \frac{\int F_D(\nu)\epsilon_A(\nu)d\nu}{\int F_D(\nu)d\nu \int \epsilon_A(\nu)d\nu} \qquad (13)$$

where H^0_{DA} is a matrix element describing the electronic coupling between D and A at contact distance R_0 and β_{EET} is a constant which depends on the nature of the spacer and which accounts for the fall off the D−A electronic interaction with distance.

EET via the Dexter mechanism is a TB process, whose efficiency is mainly controlled by the orbital overlap and by the nature of the spacer.

Calculation of k_E requires the knowledge of both H^0_{DA} and β_{EET}, which are not readily accessible. On the other hand, the calculation of k_C using eq 11 is straightforward as long as the emission and absorption spectra of D and A and the geometry of the arrays are known. The spectral overlap integrals J_F and the orientation factors κ for arrays that do not contain NiTPP are listed in Table 3.

The rate constants for Förster EET calculated using eq 11 are listed in Table 4. As the first absorption band of ZnTPP is due to two degenerate excited states with two separate transition dipoles, there are four different dipole−dipole interactions involved in the EET between two ZnTPP chromophores. For the calculation of k_C, the average value of κ^2 was used (see Table 3). In compound **9**, six different relative geometries of the ZnTPP chromophores have to be considered. The resulting rate constants are listed in Table 4 for the D_{2d} structure. For EET between ZnTPP and FbTPP moieties and between two FbTPP chromophores, the average over the four κ^2 was also used. This is in principle not strictly correct, as the Q_x and Q_y transition dipoles are not degenerate in FbTPP. However, polarization measurements have shown that the short wavelength Q bands of FbTPP cannot be associated with a single transition dipole.

By comparing the k_C and k_{EET} values listed in Table 4, it appears that the dipole−dipole interaction as expressed by eq 11 does not completely account for the observed EET rate constants. A possible reason for this difference could be the occurrence of higher order multipole interactions. Chang has shown that their neglect could lead to an underestimation of k_C when the center to center distance R is of the same order of magnitude as the diameter of the chromophore.[54] According to this author, multipole interactions can enhance the EET between chlorophyll molecules by a factor of 2 with $R \approx 12$ Å. In the arrays investigated here, the shortest R amounts to 23 Å, thus, the contribution of these higher order Coulombic interactions should not lead to a significant increase of k_C. Consequently, the difference observed for the trimers and the hexamer can be ascribed to the contribution of the exchange mechanism. A similar observation has been reported by Hsiao et al.[11] for dyads composed of ZnTPP and FbTPP with a distance R of 20 Å. In this case, the observed EET rate constants were more than 20 times faster than the calculated k_C. It was concluded that EET was basically a TB process.

Table 4 shows the rate constants for EET via the exchange mechanism, calculated as $k_E = k_{EET} - k_C$. For the hexamer **8**, this rate constant was calculated using eq 10. Table 1 shows that the ratio of the TS to TB distances are identical for all trimers. However, the k_E/k_C ratio changes dramatically with the absolute interchromophoric distance. At short distance, EET occurs via both Coulombic and exchange interaction. However at larger distances, the TB process dominates. Finally for the hexamer **8**, where the TB distance is twice as large as the TS distance, both interactions are of the same order of magnitude.

According to eq 13, k_E should exhibit an exponential decrease with increasing distance when all other parameters are kept constant. Figure 8A shows the logarithmic plot of k_E determined as described above as a function of the TB distance. The points correspond to ZnTPP/ZnTPP as well as ZnTPP/FbTPP EET, for which the spectral overlap integrals and H^0_{DA} are similar. Indeed, according to Lindsey and co-workers TB EET in ZnTPP/ZnTPP and ZnTPP/FbTPP dyads proceeds with almost the same rate constant.[55] A linear regression with this data results in a slope of 0.15 Å^{-1}. This value corresponds to the constant β_{EET} in eq 13 and is a measure of the electronic conductivity of the

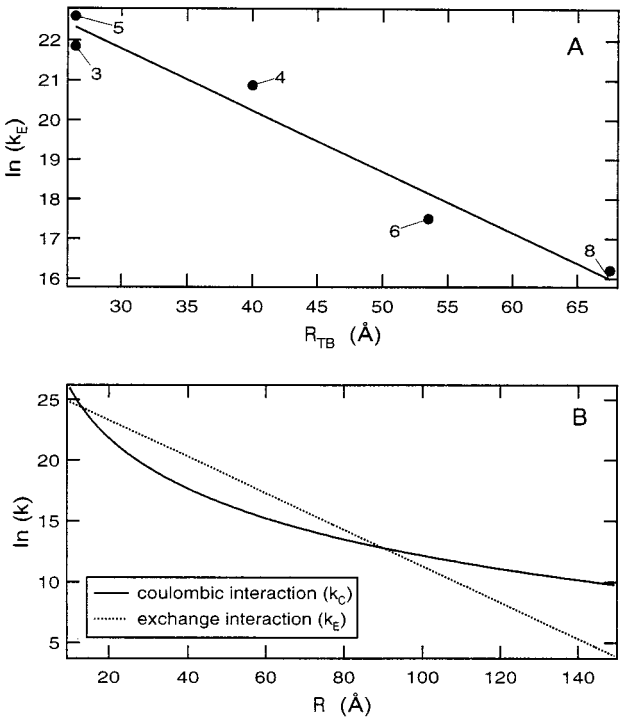

Figure 8. (A) Logarithmic plot of the rate constant of EET via the exchange mechanism as a function of the TB distance. (B) Distance dependence of the contributions of Coulombic and exchange interactions to EET.

spacer. The β_{EET} value obtained here indicates that the phenylethynyl spacer is a good conductor. As a comparison, Closs and co-workers have measured a value of β_{EET} of 1.7 Å^{-1} for the triplet energy transfer between D and A separated by 1,4-cyclohexanediyl spacers.[56] The distance dependence of electron transfer (ET) reactions is also characterized by a parameter β_{ET}.[57] Closs and co-workers have shown that $\beta_{EET} \approx 2\beta_{ET}$.[56] This was explained by the fact that EET via the exchange mechanism is a double ET. This relationship can be used to estimate β_{EET} from β_{ET}, as the distance dependence of intramolecular ET is well documented. Intramolecular ET within organic molecules, metal complexes, proteins as well as intermolecular ET in glasses has been reported to exhibit a distance dependence with a β_{ET} value in the range of 0.7−1.4 Å^{-1}.[58,59] Therefore, TB EET should certainly not occur in porphyrin arrays with saturated linkers. For example, k_E calculated with $\beta_{EET} = 1$ Å^{-1} amounts to 0.3 s^{-1} for compound **3**!

The exponential fall off of k_E with distance as determined in this study supports the estimation of the relative contributions of TS and TB interactions to the EET listed in Table 4.

Figure 8B shows the distance dependence of k_C and k_E calculated with eq 11 and the parameters obtained from the fit in Figure 8A, respectively. This plot confirms that, at short distances, TS interaction dominates. Because TB interaction has a weaker distance dependence than TS interaction, EET proceeds mostly via the Dexter mechanism at distances ranging from 20 to about 50 Å. Finally, at longer distances, both processes become very slow, although TS interaction becomes dominant again. In the molecules studied here, it should not be forgotten that the TB and TS distances are not equal (see Table 1).

Table 4 shows the six different TS k_C for the tetramer **9** in the D_{2d} structure. From the two different TS distances (see Table 1), one could have expected two large and four smaller rate constants. In this case, the anisotropy would have followed a double exponential decay as discussed above (see eq 8). However, the calculated rate constants cannot be easily sorted into two distinct groups and therefore the decay of the anisotropy was simulated using the six calculated rate constants. The simulated decay fits a single exponential function very well but the resulting decay time depends on which of the four ZnTPP chromophores is initially excited. These decay times are 500 ps, 444 ps, 392 ps, and 376 ps for initial excitation on P_1, P_2, P_3, and P_4, respectively. As each of these four chromophores has the same probability to be initially excited, the average of the four decays has to be considered. This results in an anisotropy decay of 427 ps, i.e., about 3 times longer than the measured one. The k_C values calculated assuming the optimal average orientational factor for each chromophore pairs are still too small by a factor of about 2 for both D_{2d} and S_4 structures.

The occurrence of TB EET in this molecule is questionable. Indeed, the presence of the central saturated carbon atom must strongly affect the conductivity of the spacer.

As mentioned above, the β_{EET} value for saturated hydrocarbon spacers has been determined to be around 1.7 Å^{-1}. If one calculates k_E with the parameters determined from the plot of Figure 8A, using 29 Å with $\beta_{EET} = 0.15$ Å^{-1} and 3 Å with $\beta_{EET} = 1.7$ Å^{-1}, a value of $2 \cdot 10^7$ s^{-1} is obtained. To account for the difference between the measured k_{EET} and the calculated k_C, k_E should be 60 times higher. This would be only possible if the β_{EET} value for the single bond to the central carbon atom were equal to 0.3 Å^{-1}. Figure 7C shows that, in the D_{2d} geometry, some TS coupling between two phenyl rings adjacent to the central carbon atom could somewhat improve the conductivity of the spacer. It is however doubtful that this coupling is strong enough to decrease β_{EET} sufficiently.

A possible reason for the difference between the calculated and observed rate constants could be that the actual structure of compound **9** is different from the calculated ones. Indeed, according to the calculated structures, the anisotropy should decay from 0.1 to 0.028 or 0.023. However, the anisotropy was measured to decay down to zero. As the energy minimum is very shallow, especially for a torsion around the bond connecting the porphyrin to the spacer, the geometry of this floppy molecule at room temperature and in solution is probably not well defined. A distribution of different geometries could explain the very small r_f measured with this compound. However, the fact that the k_C values calculated with optimal orientational factors are still too small, indicates that differences between the actual and the calculated torsion angle cannot entirely explain the discrepancy between the measured and the calculated EET rate constants. This difference might be due to a smaller TS distance between the ZnTPP moieties. With a κ^2 of 1.5, the measured k_{EET} is reproduced with $R_{TS} = 22$ Å. Some bending the branches of compound **9** could lead to a reduction of the TS distance. As the distance between the central carbon and the a Zn atom amounts to 16.1 Å and as the spacers are not perfectly rigid, a decrease of the TS distance of 4−5 Å upon large amplitude motion of the branches is not physically unrealistic. Of course, such motion also takes place with the trimers, but this effect should only be significant for molecules with long branches, i.e., for compounds **4** and **6**. However, EET in this arrays is dominated by the exchange interaction which is not affected by the TS distance.

In summary, there is clearly not a single EET rate constant for compound **9**. Consequently, the value of $k_{obs}/4$ can be considered as an average EET rate constant. Although this value is substantially larger than the calculated one for TS EET, it is nevertheless highly probable that EET predominantly proceeds via the Förster mechanism.

Conclusion

These investigations have shown that both the Coulombic and the exchange interactions are operative in these porphyrin arrays. Thus, both channels can be optimized to further enhance the EET efficiency. The distance is a crucial parameter: the present results show that a reduction of the TS distance should strongly accelerate EET via the Förster mechanism. A shortening of the TB distance should have a somewhat smaller effect on the exchange interaction. This is due to the good conducting property of the spacer, which actually acts as a wire. A better wire could lead to a strong electronic interaction between the chromophores via exciton coupling. The choice of the chromophore is of course very crucial for an efficient antenna. An important parameter is the excited state lifetime of the energy donor. Although EET between two ZnTPP moieties is about 4 times faster than EET between two FbTPP, the EET efficiency is higher in the second case, because of the longer excited lifetime of FbTPP. For the same reason, chromophores like NiTPP should absolutely be avoided.

Acknowledgment. This work was supported by the Fonds National Suisse de la Recherche Scientifique through Projects 20-49235.96, 21-49521.96, and 20-053568.98 and by the programme d'encouragement à la relève universitaire de la Confédération. Financial support from the Fonds de la recherche and the Conseil de l'Université de Fribourg is also acknowledged. NMR spectra on the Bruker Avance DRX 500 instrument were measured by F. Fehr and mass spectra by F. Nydegger and I. Müller.

Supporting Information Available: Synthesis and characterization of all new compounds. Supporting Information is available free of charge via the Internet at http://pubs.acs.org.

References and Notes

(1) Gust, D.; Moore, T. A.; Moore, A. L. *Acc. Chem. Res.* **1993**, *26*, 198.
(2) Wasielewski, M. R. *Chem. Rev.* **1992**, *92*, 435.
(3) Sundström, V.; vanGrondelle, R.; denHollander, W. T. F. *Biochim. Biophys. Acta* **1986**, *851*, 431.
(4) Schatz, G. H.; Brock, H.; Holtzwarth, A. R. *Proc. Natl. Acad. Sci. U.S.A.* **1987**, *84*, 8414.
(5) Du, M.; Xie, X.; Jia, Y.; Mets, L.; Fleming, G. R. *Chem. Phys. Lett.* **1993**, *201*, 535.
(6) vanGrondelle, R.; Dekker, J. P.; Gillbro, T.; Sundström, V. *Biochim. Biophys. Acta* **1994**, *1187*, 1.
(7) Tabushi, I.; Sasaki, T. *Tet. Lett.* **1982**, *23*, 1913.
(8) Nagata, T. *Bull. Chem. Soc. Jpn.* **1991**, *64*, 3005.
(9) Gust, D.; Moore, T. A.; Moore, A. L.; Gao, F.; Luttrull, D.; DeGraziano, J. M.; Ma, X. C.; Makings, L. R.; Lee, S.-J.; Trier, T. T.; Bittersmann, E.; Seely, G. R.; Woodward, S.; Bensasson, R. V.; Rougée, M.; DeSchryver, F. C.; VanderAuweraer, M. *J. Am. Chem. Soc.* **1991**, *113*, 3638.
(10) Prathapan, S.; Johnson, T. E.; Lindsey, J. S. *J. Am. Chem. Soc.* **1993**, *115*, 7519.
(11) Hsiao, J. S.; Krueger, B. P.; Wagner, R. W.; Johnson, T. E.; Delaney, J. K.; Mauzerall, D. C.; Fleming, G. R.; Lindsey, J. S.; Bocian, D. F.; Donohoe, R. J. *J. Am. Chem. Soc.* **1996**, *118*, 11181.
(12) Overfield, R. E.; Scherz, A.; Kaufmann, K. J.; Wasielewski, M. R. *J. Am. Chem. Soc.* **1983**, *1983*, 4256.
(13) Mialocq, J. C.; Giannotti, C.; Maillard, P.; Momenteau, M. *Chem. Phys. Lett.* **1984**, *112*, 87.
(14) Brookfield, R. L.; Ellul, H.; Harriman, A.; Porter, G. *J. Chem. Soc., Faraday Trans. 2* **1986**, *82*, 219.
(15) Beljonne, D.; O'Keefe, G. E.; Hamer, P. J.; Friend, R. H.; Anderson, H. L.; Bredas, J. L. *J. Chem. Phys.* **1997**, *106*, 9439.
(16) Lin, V. S.-Y.; Therien, M. J. *Chem. Eur. J.* **1995**, *1*, 645.
(17) Arnold, D. P.; Heath, G. A. *J. Am. Chem. Soc.* **1993**, *115*, 12197.
(18) Kumble, R.; Palese, S.; Lin, V. S. Y.; Therien, M. J.; Hochstrasser, R. M. *J. Am. Chem. Soc.* **1998**, *120*, 11489.
(19) Scholes, G. D.; Ghiggino, K. P.; Oliver, A. M.; Paddon-Row, M. N. *J. Phys. Chem.* **1993**, *97*, 11871.
(20) Kroon, J.; Oliver, A. M.; Paddon-Row, M. N.; Verhoeven, J. W. *J. Am. Chem. Soc.* **1990**, *112*, 4868.
(21) Mongin, O.; Gossauer, A. *Tetrahedron Lett.* **1996**, *37*, 3825-3828.
(22) Mongin, O.; Gossauer, A. *Tetrahedron* **1997**, *53*, 6835-6846.
(23) Mongin, O.; Papamicaël, C.; Hoyler, N.; Gossauer, A. *J. Org. Chem.* **1998**, *63*, 5568.
(24) Hübel, W. R. M. *Angew. Chem.* **1962**, *74*, 781.
(25) Vauthey, E.; Henseler, A. *J. Phys. Chem.* **1995**, *99*, 8652.
(26) Högemann, C.; Pauchard, M.; Vauthey, E. *Rev. Sci. Instrum.* **1996**, *67*, 3449.
(27) Gumy, J.-C.; Vauthey, E. *J. Phys. Chem.* **1996**, *100*, 8628.
(28) Dewar, M. J. S.; Zoebisch, E. G.; Healy, E. F.; Stewart, J. J. P. *J. Am. Chem. Soc.* **1985**, *107*, 3902.
(29) Frisch, M. J.; Trucks, G. W.; Schlegel, H. B.; Gill, P. M. W.; Johnson, B. G.; Robb, M. A.; Cheeseman, J. R.; Keith, T.; Petersson, G. A.; Montogomery, J. A.; Raghavachari, K.; Al-Laham, M. A.; Zakrzewski, V. G.; Ortiz, J. V.; Foresman, J. B.; Cioslowski, J.; Stefanov, B. B.; Nanayakkara, A.; Challacombe, M.; Peng, C. Y.; Ayala, P. Y.; Chen, W.; Wong, M. W.; Andres, J. L.; Repogle, E. S.; Gomperts, R.; Martin, R. L.; Fox, D. J.; Binkley, J. S.; DeFrees, D. J.; Baker, J.; Stewart, J. P.; Head-Gordon, M.; Gonzales, M. C.; Pople, J. A. *Gaussian 94*, Revision E2; Gaussian, Inc.: Pittsburgh, 1995.
(30) Becke, A. D. *J. Chem. Phys.* **1993**, *98*, 5648.
(31) Lee, C.; Yang, W.; Parr, R. G. *Phys. Rev. B* **1988**, *37*, 785.
(32) Johnson, B. G.; Gill, P. M. W.; Pople, J. A. *J. Chem. Phys.* **1993**, *98*, 5612.
(33) Antipas, A.; Gouterman, M. *J. Am. Chem. Soc.* **1983**, *105*, 4896.
(34) Kim, D.; Kirmaier, C.; Holten, D. *Chem. Phys.* **1983**, *75*, 305.
(35) Davila, J.; Harriman, A.; Milgrom, L. R. *Chem. Phys. Lett.* **1987**, *136*, 427.
(36) Fayer, M. D. *Ann. Rev. Phys. Chem.* **1982**, *33*, 63.
(37) Eichler, H. J.; Günter, P.; Pohl, D. W. *Laser-Induced Dynamic Gratings*; Springer Verlag: Berlin, 1986.
(38) Kogelnik, H. *Bell. Syst. Tech. J.* **1969**, *48*, 2909.
(39) Högemann, C.; Vauthey, E. *Isr. J. Chem.* **1998**, *38*, 181.
(40) Rodriguez, J.; Kirmaier, C.; Holten, D. *J. Am. Chem. Soc.* **1989**, *111*, 6500.
(41) Nishino, N.; Wagner, R. W.; Lindsey, J. S. *J. Org. Chem.* **1996**, *61*, 7534.
(42) Rodriguez, J.; Holten, D. *J. Chem. Phys.* **1989**, *91*, 3525.
(43) Eyring, G.; Fayer, M. D. *J. Chem. Phys.* **1984**, *81*, 4314.
(44) Fourkas, J. T.; Trebino, R.; Fayer, M. D. *J. Chem. Phys.* **1992**, *97*, 69.
(45) Myers, A. B.; Hochstrasser, R. M. *IEEE J. Quantum Electron.* **1986**, *QE-22*, 1482.
(46) Wynne, K.; Hochstrasser, R. M. *Chem. Phys.* **1993**, *171*, 179.
(47) Schlabach, M.; Wehrle, B.; Rumpel, H.; Braun, J.; Scherer, G.; Limbach, H. H. *Ber. Bunsen-Ges. Phys. Chem.* **1992**, *96*, 821.
(48) Borisevich, E. A.; Egorova, G. D.; Knyukshto, V. N.; Solovev, K. N. *Opt. Spectrosc.* **1986**, *60*, 454.
(49) Brodard, P.; Vauthey, E. *Chem. Phys. Lett.* In print.
(50) Förster, T. *Discuss. Faraday Soc.* **1959**, *27*, 7.
(51) Quimby, D. J.; Longo, F. R. *J. Am. Chem. Soc.* **1975**, *97*, 5111.
(52) Seybold, P. G.; Gouterman, M. *J. Mol. Spectrosc.* **1969**, *31*, 1.
(53) Dexter, D. L. *J. Chem. Phys.* **1953**, *21*, 836.
(54) Chang, J. C. *J. Chem. Phys.* **1977**, *67*, 3901.
(55) VanPatten, P. G.; Shreve, A. P.; Lindsey, J. S.; Donohoe, R. J. *J. Phys. Chem. B* **1998**, *102*, 4209.
(56) Closs, G. L.; Piotrowak, D.; MacInnis, J.; Fleming, G. R. *J. Am. Chem. Soc.* **1988**, *110*, 2652.
(57) Marcus, R. A.; Sutin, N. *Biochim. Biophys. Acta* **1985**, *811*, 265.
(58) Barbara, P. F.; Meyer, T. J.; Ratner, M. A. *J. Phys. Chem.* **1996**, *100*, 13148.
(59) Ratner, M. A.; Jortner, J. In *Molecular Electronics*; Ratner, M. A., Jortner, J., Eds.; Blackwell Science, Inc.: Oxford, 1997; pp 5.